JOURNAL OF GEOPHYSICAL RESEARCH, VOL. 113, E08013, doi:10.1029/2007JE002993, 2008

Internal structure of Mercury: Implications of a molten core

M. A. Riner,[1] C. R. Bina,[2] M. S. Robinson,[1] and S. J. Desch[1]

Received 20 August 2007; revised 26 March 2008; accepted 22 April 2008; published 15 August 2008.

[1] Mercury is unique among the terrestrial planets for its relatively low mass (3.302×10^{23} kg) and high average density (5.427 g cm^{-3}) that together imply an unusual iron-rich bulk composition and thus provide an important constraint on planet formation and evolution and on compositional variations between the planets. In light of the recent discovery of a partially or fully molten core of Mercury, we model plausible interior density structures of Mercury using layered cores and the elastic properties of molten core materials. We present constraints on Mercury's decompressed density, composition, and interior structure, including elucidation of assumptions and methodology. We demonstrate the importance of molten and/or layered cores to accurately model Mercury's interior and to correctly interpret anticipated spacecraft geophysical observations. The core radius and core mass fraction will be tightly constrained by Earth-based radar and anticipated spacecraft tracking observations, but the bulk core sulfur content and extent of the molten core are less well constrained. Finally, we discuss the implications of incorporating molten materials in modeled density structures on the hypotheses of Mercury's iron enrichment and on anticipated spacecraft results.

Citation: Riner, M. A., C. R. Bina, M. S. Robinson, and S. J. Desch (2008), Internal structure of Mercury: Implications of a molten core, *J. Geophys. Res.*, *113*, E08013, doi:10.1029/2007JE002993.

1. Introduction

[2] The high iron content of Mercury, inferred from its relatively low mass and high average density (Table 1), provides an important constraint for the initial temperature of the solar nebula, the degree of radial mixing, and the extent of condensation and evaporation [e.g., *Wetherill*, 1994]. The high iron content of Mercury could be the result of chemical and thermal gradients in the solar nebula or partial removal of the silicate portion of a differentiated planet by giant impact or vaporization [*Benz et al.*, 1988; *Cameron*, 1985; *Fegley and Cameron*, 1987; *Kortenkamp et al.*, 2000; *Lewis*, 1988; *Weidenschilling*, 1978; *Weidenschilling and Cuzzi*, 1993; *Wetherill*, 1988, 1994]. These hypotheses lead to different predictions of the bulk chemistry of Mercury, particularly the abundance of volatile elements [e.g., *Taylor and Scott*, 2003].

[3] Meaningful interplanetary comparisons of bulk composition inferred from bulk density require the removal of self-compression effects. Decompressed densities (density of a planet at standard temperature and pressure, STP, here defined as 0.1 MPa, 300 K) are commonly cited in the scientific literature (Table 1) and provide first-order information concerning bulk silicate to metal ratios [*Wasson*, 1988]. However, details of the methodologies and assumptions concerning such calculations are not well documented thus making assessments of their accuracies problematic.

[4] Detailed knowledge of Mercury's composition can be used to distinguish between different iron enrichment hypotheses. However, little is directly known about Mercury's composition. Compositional inferences have been made on the basis of Mercury's high mean density, surface spectral observations, the composition of the exosphere, the amplitude of the forced physical librations, and the presence of an intrinsic magnetic field. The iron enrichment of Mercury was postulated as early as 1951 when Urey estimated that 63% of Mercury's mass is iron-nickel metal. Subsequent models of Mercury's interior suggest a pure iron core of at least 60 to 70% of the total mass [*Basaltic Volcanism Study Project (BVSP)*, 1981; *Harder and Schubert*, 2001; *Kozlovskaya*, 1969; *Reynolds and Summers*, 1969; *Siegfried and Solomon*, 1974]. Mercury's core could be larger if, like the Earth's core, it contains one or more light alloying elements [*Harder and Schubert*, 2001].

[5] Spectral properties of the surface of Mercury imply a crustal FeO less than 6 wt% [*McCord and Clark*, 1979; *Vilas*, 1988] and most likely less than 3 wt% [*Blewett et al.*, 1997; *Robinson and Lucey*, 1997]. From spectral parameters derived from Mariner 10 color image data, *Robinson and Lucey* [1997] noted that the smooth plains differ little from the crustal average. Because the smooth plains are thought to be volcanic flows and FeO has a partition coefficient near one, *Robinson and Taylor* [2001] inferred that magma source regions (upper mantle) have an FeO equivalent to that of the crust: $\lesssim$3 wt%. The existing indirect evidence indicates that Mercury's bulk silicate is depleted in FeO relative to the other terrestrial planets.

[1] School of Earth and Space Exploration, Arizona State University, Tempe, Arizona, USA.
[2] Department of Earth and Planetary Sciences, Northwestern University, Evanston, Illinois, USA.

0148-0227/08/2007JE002993$09.00

Table 1. Constraints on the Interiors of the Terrestrial Planets

	Mass (kg)[a]	Radius (km)[a]	Average Density (g cm^{-3})[a]	Decompressed Density (g cm^{-3})	C/MR[b]
Mercury	3.302×10^{23}	2440	5.427	5.3[b]	
Venus	4.869×10^{24}	6051	5.245	3.95–4.0[c] or 4.4[d]	
Earth	5.974×10^{24}	6371	5.514	4.0–4.05[c] or 4.45[d]	0.3315 ± 0.0000[a]
Moon	7.348×10^{22}	1738	3.344	3.3[e]	0.391 ± 0.002[a]
Mars	6.419×10^{23}	3390	3.934	3.7–3.85[f]	0.3635 ± 0.0012[g]

[a]See *BVSP* [1981, Table 4.2.1, and references therein].
[b]*Lewis* [1988], *Wasson* [1988], *BVSP* [1981], *Lewis* [1972], and *Goettel* [1988].
[c]*Lewis* [1988], *Wasson* [1988], and *Goettel* [1988].
[d]*Urey* [1951] and *Lewis* [1972].
[e]*BVSP* [1981] and *Wasson* [1988].
[f]*Lewis* [1972], *Lewis* [1988], *Wasson* [1988], and *Goettel* [1988].
[g]*Folkner et al.* [1997].

[6] Mercury's volatile content is simply not known. Sodium and potassium are present in the exosphere of Mercury [*Potter and Morgan*, 1985, 1986], but it is not clear if the source of these volatiles is endogenic or exogenic. Equilibrium condensation models suggest Mercury is depleted in volatiles, but Mercury could have formed from planetesimals from a wide zone in the solar nebula [*Wetherill*, 1994] and could be volatile-rich.

[7] Recent Earth-based radar measurements of subtle deviations from the mean resonant spin rate of Mercury show that the mantle of Mercury is decoupled from a core that is at least partially molten [*Margot et al.*, 2007]. As Mercury orbits the Sun it experiences reversing torques due to variations in the Sun's gravitational influence on the asymmetrical planet. These torques affect the spin rate of the planet and the resulting oscillations in longitude are called forced librations. The magnitude of the forced librations depends on the state of the core [*Peale*, 1976]. A molten core is decoupled from the mantle and does not follow the librations while for a solid core the entire planet participates in the librations. The amplitude of the librations for a liquid core should be twice as great as that for a solid core. The magnitude of the forced librations of Mercury, together with the Mariner 10 value of the gravitational harmonic coefficient C_{22} indicate that Mercury's core is at least partially molten [*Margot et al.*, 2007]; however, the ratio of molten to solid material is not yet constrained.

[8] Mercury has an intrinsic magnetic field [*Ness et al.*, 1974], but the origin is not understood [*Stevenson*, 2003]. Suggested explanations of Mercury's magnetic field include a hydromagnetic dynamo, a strong remnant field, or thermoelectric dynamo [*Aharonson et al.*, 2004; *Giampieri and Balogh*, 2002; *Schubert et al.*, 1988; *Srnka*, 1976; *Stephenson*, 1976; *Stevenson*, 2003]. Numerical simulations have shown that a variety of dynamo geometries can produce the observed magnetic field [*Christensen*, 2006; *Heimpel et al.*, 2005; *Stanley et al.*, 2005]. The hydromagnetic dynamo possibility led many researchers to postulate that Mercury has a molten outer core [*Ness et al.*, 1974; *Stevenson et al.*, 1983]. Even so, the discovery of a molten core in Mercury is surprising. A molten outer core implies a light alloying element in the core to lower the melting temperature of iron [*Schubert et al.*, 1988; *Siegfried and Solomon*, 1974; *Solomon*, 1976] and thus is at odds with refractory models of Mercury.

[9] If a hydromagnetic dynamo generates Mercury's magnetic field, the sulfur content of the core might be constrained. The conditions required for an active dynamo are not known. Thin shell configurations, with molten outer cores as small as 100–200 km deep, have been explored and may produce the observed Mercurian magnetic field. Thermal models indicate that the core sulfur content must be at least 0.1 wt% for an outer core to remain liquid to the present time [*Schubert et al.*, 1988]. Numerical models indicate that thermal convection in Mercury's core is not likely, and compositional convection, from release of S as Fe crystallizes into the inner core, is required to explain a dynamo origin of the magnetic field [*Hauck et al.*, 2004; *Schubert et al.*, 1988; *Stevenson et al.*, 1983]. A bulk core sulfur content greater than 7–10% precludes the formation of a solid inner core; thus if a hydromagnetic dynamo causes the magnetic field, then the bulk core sulfur content is likely between 0.1 and 10 wt% [*Hauck et al.*, 2004; *Schubert et al.*, 1988; *Stevenson et al.*, 1983].

[10] Early models of Mercury's interior were based on the total mass, total radius, and cosmochemical arguments of plausible planet compositions [*BVSP*, 1981; *Kozlovskaya*, 1969; *Reynolds and Summers*, 1969; *Siegfried and Solomon*, 1974]. None of these models considered fully or partially molten cores, layered cores, or cores with a light alloying element. These early models either considered cold, solid, pure Fe (or Fe-Ni) cores or homogeneous, iron-enriched planets without cores. These models laid a solid groundwork establishing the lower estimate on the size of Mercury's core and generally agreed that the core of Mercury is 60–70% of its total mass.

[11] None of these models explicitly calculated the decompressed density for differentiated models, but we can estimate a decompressed density from their models if they present the mass and zero-pressure density of each layer (i.e., mantle and core). We calculate the zero-pressure volume of each layer from the given mass and zero-pressure density and divide the total planet mass by the sum of the zero-pressure volume of all layers (Table 2). These values can then be compared to the results of our model.

[12] *Harder and Schubert* [2001] presented new models for the interior of Mercury and were the first to consider the effect of a light alloying element on the density structure of Mercury. At that time, experimental data for liquid Fe alloys were not available at the appropriate temperatures and pressures, so *Harder and Schubert* [2001] considered solid cores from pure Fe to pure FeS (27.5 wt% S) and argued that density changes due to melting are much smaller than density differences due to compositional variations. Their

Table 2. Our Estimates of the Decompressed Density From Previously Published Models of Mercury[a]

Reference	Decompressed Density (g cm^{-3})	Comments
Reynolds and Summers [1969]	5.2	Max. Fe metal, no Fe oxide
	5.4	Min. Fe metal, max Fe oxide
	5.3	Intermediate model with Fe metal and Fe oxide, assumes efficient core forming processes
BVSP [1981]	5.4–5.5	Models Me-1 through Me-5
Kozlovskaya [1969]	5.0	All metal in the core. We assume zero-pressure core density 7.9 g cm^{-3}
Siegfried and Solomon [1974]	5.15	Homogeneous planet, no core, explicitly calculated by *Siegfried and Solomon* [1974]
	5.3	Our estimated value for their differentiated model, assuming zero-pressure core density of 7.9 g cm^{-3}.

[a]In all cases we used the value of the total mass of Mercury cited in the original paper. We used the zero-pressure densities of each layer when given in the reference and indicate those cases in which we assumed a zero-pressure density. We did not include the decompressed density for homogenous models (those without cores) because we find such a model improbable. We include *Siegfried and Solomon*'s [1974] homogeneous Mercury decompressed density estimate because, to our knowledge, it is the only explicitly calculated decompressed density in the literature.

model results have cores 1780–2440 km in radius (73–100% of the total radius) with the smallest cores being pure Fe and the largest cores pure FeS. They found that the model was insensitive to relatively large uncertainties in the mantle density and temperature and that the normalized moment of inertia, when measured would put tight constraints on the radius and density of the core. However, the correlation of core radius/density to the normalized moment of inertia is likely sensitive to the assumption of a single layer core, and *Spohn et al.* [2001] assert that the normalized moment of inertia will not significantly constrain models of Mercury with layered cores. Here the term "layered core" refers to a molten inner and solid outer core, possibly with different compositions, and not to the discrete shells used to numerically model the core.

[13] Additional constraints on the composition and interior structure of Mercury will come from spacecraft missions to the planet. The only spacecraft to visit Mercury, Mariner 10, flew by the planet three times in 1974–1975. The Mercury Surface, Space Environment, Geochemistry, and Ranging (MESSENGER) mission will fly by Mercury three times (2008–2009) and become the first spacecraft to orbit Mercury (2011) [see *Solomon et al.*, 2001]. The European Space Agency's BepiColombo mission is scheduled to orbit Mercury beginning in 2019. These missions will take measurements to better characterize the composition and evolution of the surface and the exosphere. Detailed gravity tracking of orbiting spacecraft will allow for improved determination of the gravitational coefficients C_{22} and J_2. Together with radar-determined values of the obliquity and the librations [*Margot et al.*, 2007], the normalized moment of inertia, C/MR^2, and ratio of the moment of inertia of the mantle to that of the whole planet, C_m/C, can be determined where C is the moment of inertia about the rotation axis, M is the total planet mass, and R is the total planet radius. The normalized moment of inertia describes the radial concentration of mass. A normalized moment of inertia of 0.4 describes a homogeneous sphere. Values less than 0.4 describe planets with increasing concentration of mass toward the center of the body. The moment of inertia of the mantle relative to the whole planet's moment of inertia can be determined because the core is decoupled from the mantle and does not follow the 88-day physical libration of the mantle [*Margot et al.*, 2007; *Peale et al.*, 2002].

[14] Until recently, the only considerations of layered Mercurian cores (inner and outer cores) utilize constant density models which assume the density within each layer (mantle, outer core, and inner core) does not change with depth due to self-compression [*Spohn et al.*, 2001; *Van Hoolst and Jacobs*, 2003]. These simple models were used to assess the constraints of gravity measurements from BepiColombo [*Spohn et al.*, 2001] or to estimate the sensitivity of tides to the interior structure [*Van Hoolst and Jacobs*, 2003] but not to explore the full range of plausible density structures. Neither study considered the effect of sulfur or melting on the elastic properties of the core. *Van Hoolst and Jacobs* [2003] incorporated a density decrease due to melting, as a constant percentage of the solid density, on the basis of experimental data of pure iron. Changes in elastic properties due to melting were not included, and density changes due to melting in Fe alloys were assumed to be identical to density changes due to melting of pure Fe. They note that incorporating the effects of melting on the density of core materials results in larger core radii for a given core sulfur content than determined by *Harder and Schubert* [2001] and *Spohn et al.* [2001].

[15] The recent discovery of Mercury's partially or fully molten core [*Margot et al.*, 2007] along with new high-pressure experimental results [*Balog et al.*, 2003; *Sanloup et al.*, 2000] motivate new models of Mercury's interior that include molten core materials. In this study we model the interior density structure of Mercury with molten and layered cores under a range of plausible mantle, core, and thermal parameters. We present the full range of plausible decompressed densities, compositions and interior structures, discuss how spacecraft observations will constrain these ranges, and consider implications for the origin and evolution of Mercury.

2. Methods

[16] We model Mercury's interior under adiabatic compression using equations describing the mass and pressure

(equations (1)–(2)), the Adams-Williamson equation (equation (3)) with the third-order Birch-Murnaghan finite strain equation of state (equation (4)) [e.g., *Davies and Dziewonski*, 1975]

$$\frac{dM}{dr} = 4\pi r^2 \rho(r) \tag{1}$$

$$\frac{dP}{dr} = -\rho(r) g(r) \tag{2}$$

$$\frac{d\rho}{dr} = \frac{-GM(r)\rho(r)}{r^2 K_S} \tag{3}$$

$$K_S = K_{S0}(1+2f)^{5/2}[1 + 7f - 2\zeta f(2+9f)] \tag{4}$$

where ρ is the density, G is the universal gravitation constant, K_S is the adiabatic bulk modulus ($K_S = -\rho(dP/d\rho)_S$), r is the radius, and the zero subscript indicates zero pressure and 300 K temperature, $f = 1/2[(\rho/\rho_0)^{2/3} - 1]$, $\zeta = 3/4(4 - K_0')$, and K_0' is the pressure derivative of the bulk modulus. We integrate $d\rho/dr$ inward, using discrete 10 km thick shells, assuming g and ρ are constant within each shell.

[17] The boundary conditions are zero pressure at the surface (P(0) = 0) and the density equal to the zero-pressure, low-temperature (300 K) density at the surface ($\rho(0) = \rho_0$). Therefore we solve for ρ(P) and the temperature is not solved explicitly. We calculate the density change from zero-pressure and low-temperature density at the surface assuming an adiabatic temperature profile via the use of K_S. It is assumed that the thermal profile is adiabatic except for thermal boundary layers at the core mantle boundary (CMB) and the outer core – inner core boundary (ICB). Each thermal boundary layer is modeled as a temperature difference (ΔT) across the boundary.

[18] We model Mercury as a three-layer body: silicate mantle, molten metal outer core, and solid metal inner core. At phase or composition boundaries (CMB and ICB, generalized by the symbol B), pressures are continuous but the densities and temperatures are not continuous. We correct the STP density (solve f in equation (5) using bracketing techniques then solve for ρ) and bulk modulus (equation (4)), for adiabatic compression to the pressure (P) at the boundary. The pressure-corrected density (ρ_B) and pressure-corrected bulk modulus of the core material (K_{SB}) are corrected for the estimated temperature difference at the boundary (ΔT) (equations (6)–(7), where α is the thermal expansion coefficient, assumed to be constant with temperature, and δ_S is the second Grüneisen parameter), assuming adiabatic thermal gradients within each layer. Other models fix the temperature at the CMB or use complex thermal models sensitive to initial conditions and poorly constrained input parameters. We chose to vary ΔT as an input parameter, to accommodate large uncertainties in the interior thermal profile of Mercury. The temperature and pressure-corrected density and bulk modulus (ρ_{BT} and K_{SBT}) can then be used to apply the Adams-Williamson equation to the new region.

$$3K_{S0} f (1+2f)^{5/2}(1 - 2\zeta f) = P_B \tag{5}$$

$$\rho_{BT} = \rho_B \exp(-\alpha \Delta T) \tag{6}$$

$$K_{SBT} = K_{SB} \exp(-\alpha \Delta T) \tag{7}$$

3. Constraints and Variables

[19] Our model is constrained by the total mass (3.302×10^{23} kg) and radius (2440 km) of Mercury. We ignore the uncertainties in the total mass and total radius because they are much less significant than the uncertainties in the density profile and interior structure. The moment of inertia for Mercury is not accurately known and is thus not used as a constraint, but it is a calculated output of the model.

[20] We obtained a suite of plausible Mercury density models by systematically varying nine input parameters (mantle density, mantle bulk modulus, and pressure derivative of the mantle bulk modulus, outer and inner core radius, outer and inner core sulfur content, and temperature contrast at the CMB and ICB) within the ranges shown in Table 3. We held the thermal expansion coefficient of the outer and inner core and second Grüneisen parameter for the outer and inner core constant, as shown in Table 3. The outer core is assumed to be molten and the inner core solid. The existence and size of both the inner and outer cores are determined directly by two radii input variables, not by a thermal model and melting law. This allows full exploration of the parameter space and reflects uncertainty in the composition of Mercury's core and thermal profile but may introduce less plausible scenarios. A single-layer core of either phase is accommodated in the model by allowing the inner core radius to equal zero (all molten) or the outer and inner core radii to be equal (all solid).

[21] The model returns the pressure, bulk modulus, and density at all depths as well as the mass of each layer, the decompressed density, C/MR^2, and C_m/C. The decompressed density, whole planet moment of inertia, and mantle moment of inertia are defined by equations (8)–(10).

$$\rho^o = \frac{M_m + M_{oc} + M_{ic}}{\left(\frac{M_m}{\rho_{STPm}} + \frac{M_{oc}}{\rho_{STPoc}} + \frac{M_{ic}}{\rho_{STPic}}\right)} \tag{8}$$

$$C = \frac{8\pi}{3} \int_0^R \rho(r) r^4 dr \tag{9}$$

$$C_m = \frac{8\pi}{3} \int_{R_c}^R \rho(r) r^4 dr \tag{10}$$

where ρ^0 is the decompressed density, M is the mass, ρ_{STP} is the density at standard temperature and pressure and R is the

Table 3. Input Values for Systematic Grid Search Model of Mercury With Three Layers: Mantle, Outer Core, and Inner Core

Parameter	Range	Step Size	Description
ρ_{0m}	3.1–3.6 g cm^{-3}	0.25 g cm^{-3}	STP mantle density[a]
K_{S0m}	120–140 GPa	20 GPa	Adiabatic zero-pressure bulk modulus of the mantle[a]
K'_{S0m}	120–140 GPa	20 GPa	Pressure derivative of the adiabatic, zero-pressure bulk modulus of the mantle[a]
R_{OC}	1600–2200 km	25 km	Radius of the outer core
R_{IC}	0–R_{OC}	25 km	Radius of the inner core (restricted to $\leq R_{OC}$)
S_{OC}, S_{IC}	0–10 wt%	2%	Sulfur content of the outer core
S_{IC}	0–1/2 S_{OC} wt%	2%	Sulfur content of the inner core (restricted to $\leq$1/2 S_{OC})
α_{OC}	8.75 $\times$ 10^{-5} K^{-1}	None	Thermal expansion coefficient of the outer core[b]
α_{OC}	7.5 $\times$ 10^{-5} K^{-1}	None	Thermal expansion coefficient of the inner core[b]
Δ_{SOC}	0–1000 K	200 K	Temperature difference at CMB[c]
Δ_{SOC}	0–600 K	200 K	Temperature difference at ICB
δ_{SC}	4	None	second Grüneisen parameter for the inner and outer core[d]

[a] *Knittle* [1995].
[b] *Boehler et al.* [1990], *Fei et al.* [1995], *Urakawa et al.* [2004], *Anderson and Ahrens* [1994], *Nasch and Steinemann* [1995], and *Hixson et al.* [1990].
[c] *Ahrens et al.* [2002].
[d] *Bina and Helffrich* [1992].

radius. Results are sorted, and only those with total mass within 0.1% of Mercury's mass are considered.

[22] We neglect the presence of a crust because we allow the density of the mantle to vary within a wide range encompassing plausible silicate densities. In light of spectral evidence of low FeO in the crust and mantle of Mercury, we do not consider high-density silicates plausible, but we allow high mantle densities because there may be iron metal in the mantle if core differentiation was incomplete. We consider the mantle in our model to reflect the silicate layer of the planet with the density adjusted to reflect a volume-weighted average of the density of the crust and the density of the mantle. We neglect mantle phase transitions because the mantle in all cases is less than half the total planet mass, hence pressures in the mantle are low (<10 GPa) and significant mantle phase transitions are unlikely. Additionally, iron-rich silicates transform to high-pressure phases at lower pressures than do iron-poor silicates. Since Mercury likely has a low-FeO mantle, phase transitions in the Mercurian mantle probably occur at higher pressures than phase transitions in Earth's mantle.

[23] Mercury's core is assumed to be mostly iron since it is the most abundant high-density element in the solar system. The addition of Ni to a Fe core does not change the equation of state of iron, within the experimental uncertainties, [*Mao et al.*, 1990] and we neglect Ni in this model. For the bulk of Mercury's interior the modeled pressures and temperatures are consistent with the solid γ fcc Fe phase [*Siegfried and Solomon*, 1974].

[24] The volatile content of Mercury's core is unknown. The Earth's core is 6–10% less dense than pure iron at the appropriate temperatures and pressures of the Earth's core [*Li and Fei*, 2003, and references therein]. This density deficit has been explained by the presence of a light alloying element such as H, O, Si, S, or C [see *Li and Fei*, 2003, and references therein]. The light element composition of the Earth's core is a controversial subject (even with seismic data and a well known moment of inertia). Additional knowledge of the thermal state of the core and the equation of state of Fe alloys is needed before this issue might be resolved. Because there is a substantial body of experimental work on the Fe-S system we use sulfur as a proxy for a light alloying element in Mercury's core.

[25] Other light alloying elements, if present would change the models to some degree. Currently a complete understanding of the significance of this change is not possible without additional experimental work on the physical properties of molten Fe alloys. However, we can infer comparable density and compressibility changes for different solid Fe alloys from existing experimental data [see, e.g., *Li and Fei*, 2003]. While we expect the trends presented here to hold for other light alloying elements, the required amount of light alloying element required to produce the observed changes in density may vary by several weight percent [i.e., *Li and Fei*, 2003; *Badro et al.*, 2007].

[26] The amount of sulfur necessary to account for the observed density deficit in the Earth's outer core depends on the structure and equation of state of the alloys or compounds and is not well known. *Chen et al.* [2007] estimate 6–13 wt% S is required to explain the 6–10% density deficit for the Earth's outer core. Mercury almost certainly accreted more material from closer to the Sun than did the Earth. Therefore we consider the Earth's bulk core sulfur content as upper limit to the bulk core sulfur content of Mercury, and we limit the sulfur content of the outer core to less than 10 wt%. The crystallization of a Fe-S alloy should preferentially leave the S in the liquid phase and the quantitative details of the partitioning depend on temperature and pressure.

[27] The Earth's inner core is 1–3% lighter than pure iron, so presumably some of the light alloying element is incorporated into the solid inner core. Since we are using sulfur as a proxy for an unknown light alloying element and the partitioning behaviors of candidate light alloying elements vary, we allow some light alloying element in the solid inner core. The effects of this assumption will be discussed in the results section. We restrict the sulfur content of the inner core to less than or equal to half of the outer core sulfur content. Solid Fe-S alloys experience

Table 4. Experimental Results of the Physical Properties of Plausible Core Materials

	Material	T (K)	P (GPa)	ρ_0 (g cm^{-3})	K (GPa)	K′	A ($\times 10^{-5}$ K^{-1})
Solid	γ fcc Fe[a,b,c]	1200–2340	11–42[a]	8.2[b]	155[c]	5.5[c]	6.8[a]
	FeS IV[d]	800	10–20	4.94	54	4	6.85
Liquid	Fe (liq)[e]	1811	<200	7.019	109.7	4.66	9.2
	Fe 10%S (liq)[f]	1773–2123	<20	5.5	64.3	4.7	not available

[a]*Boehler et al.* [1990].
[b]*Boehler et al.* [1989].
[c]Values reported by *Anderson and Isaak* [2002] from fit to *Boehler et al.* [1990].
[d]*Fei et al.* [1995].
[e]*Anderson and Ahrens* [1994].
[f]*Balog et al.* [2003] and *Sanloup et al.* [2000].

several phase changes at pressures relevant to Mercury's core [*Fei et al.*, 2000]. Since the material properties are similar, we assume that the sulfur in the solid inner core occurs as the FeS IV phase [*Fei et al.*, 1995].

[28] Typically the bulk moduli of geologic materials are determined experimentally using shock wave measurements or by static compression in large-volume or diamond anvil cells. We compiled previously published bulk moduli estimates of Fe and Fe alloys, liquid and solid (Table 4). We normalized all the zero-pressure densities and bulk moduli from the experimental temperature to 300 K (using equations (4)–(5)) and, when necessary, converted isothermal bulk moduli to adiabatic bulk moduli via the relation, $K_S = K_T(1 + \alpha\gamma T)$, where γ is the Grüneisen parameter (Table 5). In the model we specify the sulfur content for the inner and outer core and calculate the density, bulk modulus and pressure derivative of the bulk modulus as a mixture of the experimentally determined values. For the solid inner core we use the Voigt-Reuss-Hill (VRH) average of the solid compositional end-members [*Watt et al.*, 1976]. The VRH average is relevant to solid materials. Because it is unclear how elastic properties of molten alloys should be averaged, we linearly interpolate between the experimental values for liquid Fe and Fe with 10 wt% S to determine the model input values for the outer core. Potential errors introduced by linear interpolation should be small, as the experimental values cover the same small compositional range we consider in the model.

[29] The experimental data on the thermal expansion of Fe alloys is limited [see *Chen et al.*, 2007, and references therein]. We ignore the temperature dependence of the thermal expansion coefficient because it has a second-order effect on the model. *Boehler et al.* [1990] determine a thermal expansion coefficient of solid γ fcc Fe of 7.7×10^{-5} K^{-1}. The thermal expansion coefficient of solid FeS IV is comparable, 6.85×10^{-5} K^{-1} at low temperature [*Fei et al.*, 1995]. We assume the addition of 10 wt% or less sulfur will result in a small decrease in the thermal expansion of γ fcc Fe and use a constant thermal expansion coefficient of 7.5×10^{-5} K^{-1} for the solid inner core. Because the thermal expansion coefficient has a second-order effect on the equation of state and because the effect of mixing on thermal expansion coefficients is unknown, we consider the thermal expansion coefficient constant for a given phase, over the compositional range 0–10 wt% sulfur. Experimental values of the thermal expansion coefficient of molten Fe in the range of $8.2–9.2 \times 10^{-5}$ K^{-1} are common [*Anderson and Ahrens*, 1994; *Hixson et al.*, 1990; *Nasch and Steinemann*, 1995]. Thermal expansion coefficients of molten Fe alloys are not known [*Sanloup et al.*, 2000]. On the basis of the small difference in the thermal expansion of solid Fe and Fe alloys [*Boehler et al.*, 1990; *Fei et al.*, 1995; *Urakawa et al.*, 2004] and following *Sanloup et al.* [2000], we assume the addition of 10 wt% or less of sulfur to molten Fe will not significantly affect the thermal expansion coefficient, and we use a constant value of 8.75×10^{-5} K^{-1} for the molten outer core.

[30] We model the thermal conditions of Mercury's interior using adiabatic temperature profiles within the mantle, outer core and inner core and temperature changes (ΔT) across the CMB and ICB. This method allows us to explore a range of possible thermal conditions and requires the fewest free parameters. We neglect the lithospheric thermal boundary layer because we do not specify any explicit temperature in the model. Thus any thermal effects due to a conductive lithosphere are taken up in the value of the zero-pressure mantle density. Assuming a thermal expansion coefficient of the order 10^{-5} K^{-1} and a temperature change across the lithosphere of the order 10^2 K [i.e., *BVSP*, 1981; *Williams et al.*, 2007], the zero-pressure mantle density changes by ~1% because of the thermal effects of the lithosphere and is easily taken up in the wide range of input mantle densities (3.1–3.6 g cc^{-1}).

[31] The minimum temperature change across the CMB and the ICB is 0 K (i.e., conductive mantle in steady state). The maximum plausible temperature change across both boundaries is harder to constrain. We estimate reasonable maximum temperature change across Mercury's CMB by

Table 5. End-Member Parameters Input Directly Into Our Model[a]

	Material	ρ_0 (g cm^{-3})	K (GPa)	K′	α (K^{-1})
Solid	γ fcc Fe[b]	8.2	158	5.5	7.5×10^{-5}
	FeS IV	5.1	62	4.0	7.5×10^{-5}
Liquid	Fe	8.0	189	4.66	8.75×10^{-5}
	Fe 10%S[c]	6.4	122	4.7	8.75×10^{-5}

[a]These values are derived from the experimental data in Table 4. All density and bulk modulus values have been normalized from the experimental temperature to 300 K and, when applicable, the bulk modulus values are corrected from isothermal (K_T) to adiabatic (K_S) via the relationship $K_s = K_T(1 - \alpha\gamma T)$. The thermal expansion values were selected by the authors and are representative values in the reported experimental range (see section 3 for additional discussion).
[b]*Anderson and Isaak* [2002] report values corrected to 300 K and we made no further temperature correction.
[c]Central experimental temperature, 1923 K, from *Balog et al.* [2003] used for correction.

Table 6. Summary of Key Output Parameters From the Model Over the Grid Search Described by Table 3[a]

Value	Full Data Set	Moderate ΔT ΔTic = 0–200 K, ΔToc = 0–600 K	Low ΔT ΔTic = 0 K, ΔToc = 0–200 K
Core radius, total (km)	1650–2075	1650–2050	1650–2025
Core radius, inner (km)	0–1850	0–1825	0–1775
Core mass fraction (%)	52–78	52–76	52–75
Outer	0–77	0–75	0–74
Inner	0–67	0–66	0–63
C/MR^2	0.319–0.353	0.319–0.352	0.319–0.351
C_m/C	0.368–0.715	0.368–0.715	0.368–0.715
$C_c/M_cR_c^2$	0.374–0.396	0.374–0.396	0.374–0.396
Decompressed density (g cm^{-3})	5.06–5.34	5.06–5.27	5.06–5.19

[a]Thermal inputs are filtered as noted in the column headings. The decompressed density is significantly affected by the thermal input values while the masses, radii of the inner and outer core and the normalized moment of inertia of the entire planet show minor affects to changes in input thermal values.

comparison to the Earth. The temperature change across the Earth's CMB is estimated to be at least 1300 K, possibly higher [*Ahrens et al.*, 2002]. Mercury is less massive than the Earth, so we expect temperatures in the interior and heat flux out of the core to be lower, but how much lower is uncertain. We select a maximum ΔT across the CMB at 1000 K.

[32] We check the reasonableness of this value by assuming the thermal boundary layer at the CMB is a conductive near surface region in which there is a significant temperature change and calculating the maximum ΔT before convection in the thermal boundary layer is predicted. We calculate the ΔT for the critical Rayleigh value, of order 1000. Assuming the mantle is heated below by a convecting molten core, the Rayleigh number is a dimensionless quantity given by equation (11) [e.g., *Turcotte and Schubert*, 2002],

$$Ra = \frac{\alpha g \rho \Delta T D^3}{\kappa \eta} \tag{11}$$

where α is the thermal expansion coefficient, g is the acceleration of gravity, ΔT is the temperature change across the thermal boundary layer, D is the thickness of the layer, κ is the thermal diffusivity and η is the reference viscosity. Combining this equation with the definition of the thermal diffusivity $\kappa = k/\rho C_p$ and the definition of heat flux $F = kdT/dx = k\Delta T/D$, where k is the thermal conductivity, ρ is the density and C_p is the heat capacity and rearranging we can solve for ΔT across the thermal boundary layer (equation (12)).

$$\Delta T = \left[\frac{Ra_{cr}\eta}{\alpha g \rho^2 C_p k^2} F^3\right]^{1/4} \tag{12}$$

[33] To estimate the maximum temperature change across the CMB we take values from *Redmond and King* [2007, Table 1] and use a heat flux of 10 mW m^{-2} [*Hauck et al.*, 2004] and find ΔT = 450 K, consistent with the results of *Williams et al.* [2007]. Given the uncertainties in the heat flux and viscosity of Mercury's mantle we use this simple exercise to constrain the magnitude of the temperature change across the CMB and consider a wide range of plausible ΔT values and explore the consequences of a range of ΔT values.

[34] The temperature across the Earth's ICB is poorly constrained, even more so for Mercury. We consider temperature changes across the ICB of 0–600 K. Rather than depend on assumptions of the composition, initial conditions and amount and distribution of radiogenic elements of Mercury we select a broad range of temperature conditions that should encompass all possible configurations of Mercury and acknowledge the significant uncertainty in these

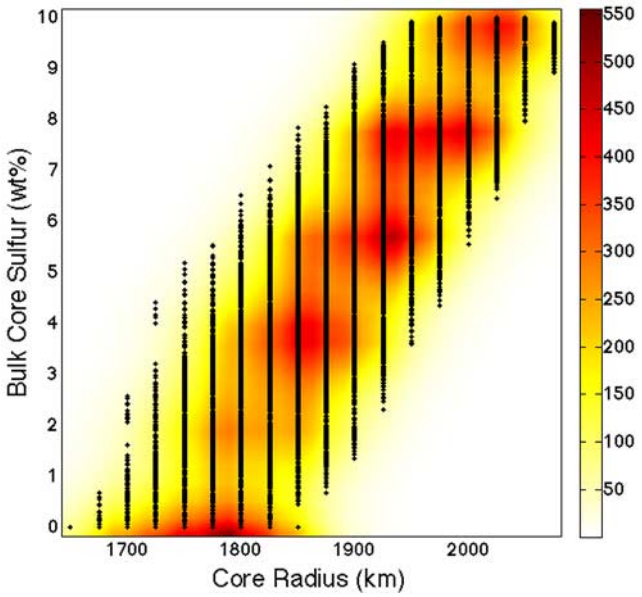

Figure 1. The core radius and bulk core sulfur content (wt%) are correlated but for a given core radius the bulk sulfur content can vary by up to 6 wt% because of variations in thermal, mantle, or core parameters. The 41,831 black points represent individual cases matching the mass of Mercury with in 0.1% and the colored background represents the number of data points in that region. The core parameters can vary even with the same core radius and sulfur content because of the variations in the distribution of mass and sulfur between the molten outer core and the solid inner core. The regular spacing of radii values for the individual data points reflects the step size used in the grid search.

Table 7. Values for the Four Example Structures Illustrated in Figure 9[a]

	Solid	Thin Shell	Traditional Dynamo	Molten
C/MR^2	0.332	0.327	0.338	0.350
C_m/C	0.688	0.602	0.535	0.418
C_c/M_cR_c	0.391	0.385	0.390	0.389
ρ^0 (g cc^{-1})	5.11	5.20	5.28	5.34
Core mass fraction	55	62	66	74
R_{OC} (km)	n/a	1800	1900	2050
R_{IC} (km)	1700	1700	950	n/a
S_{OC} (wt%)	n/a	2	4	10
S_{IC} (wt%)	0	0	0	n/a
ρ_m	3.6	3.35	3.35	3.35
K_m	120	140	100	100
K'_m	4	5	5	4
ΔT_{OC}	n/a	1000	1000	1000
ΔT_{IC}	1000	1000	1000	n/a

[a]From Figure 9: (a) single layer solid core, (b) core with a thin shell molten outer core, (c) core consistent with traditional dynamo simulations the radius of the inner core is half the total core radius, and (d) single layer, totally molten core.

values. In section 4.5 we specifically address how different thermal ranges affect our results.

4. Results

4.1. Range of Interior Structures

[35] Using a systematic grid search of input values (Table 3), our model produced over 98,000 cases within 0.1% of Mercury's mass. Given the assumptions and constraints described above, these cases describe the full range of plausible interior structures and compositions of Mercury (Table 6, column 1). The core of Mercury comprises 52–78% of the total planet mass and 68–85% of the total planet radius (1675–2075 km), compared to Earth's core which is ~32% of the total mass and ~55% of the total radius. The size of the core is most sensitive to the bulk core sulfur content (Figure 1). Even though the core size and sulfur content are correlated, there is significant scatter in the correlation due to variations in mantle, core, and thermal parameters.

[36] The mantle density does influence the interior structure of Mercury, but less so than the core properties. The interior structure and moment of inertia of Mercury are largely controlled by the core properties because in all cases the core makes up 50% or more of the total mass of the planet and because there is more variability in the core material properties (due to uncertainty in both composition and phase, and because small changes in composition have a more pronounced effect on iron alloys than on silicates). The slope of the correlation between the core radius and the normalized moment of inertia is the same, regardless of mantle density but higher mantle densities result in uniformly higher normalized moments of inertia (Figure 2). For a given core radius, the moment of inertia may vary by up to 0.025, over half the total range. If one assumes a mantle density, then the moment of inertia for a given core radius varies by less than 0.01. The mantle density has a less pronounced effect on the correlation between bulk core sulfur content and core radius. There is significant overlap in plausible values, but changes in the mantle density can influence the bulk sulfur content of a given core size by ~1.5 wt%.

4.2. Effect of Molten and Layered Cores

[37] Until recently [*Hauck et al.*, 2007], work concerning the density structure of Mercury has either neglected the effect of molten materials [*Harder and Schubert*, 2001; *Spohn et al.*, 2001] or only incorporated constant density decrease due to melting [*Van Hoolst and Jacobs*, 2003]. Experimental measurements of the physical properties of molten iron alloyed with sulfur are only recently available [*Balog et al.*, 2003; *Sanloup et al.*, 2000]. The earlier, simpler approach, while necessary at the time, neglects changes in compressibility due to melting. Melting not only decreases the density of core materials but also makes them less compressible. The magnitude of density and compressibility changes due to melting is a function of sulfur content (Figure 3).

[38] To illustrate the importance of considering phase in density models of Mercury we ran the same grid search with the input parameters described in Table 3 but replaced the liquid end-member parameters with the solid parameters in Table 5. In effect, we assumed that phase did not significantly change the density, K, and K′ of the core materials and that the solid parameters adequately describe both the inner and outer cores. Neglecting the effect of phase on the material properties of the core caused the maximum plausible core size to decrease from 2075 km to 1950 km and from 78% to 72% of the mass of the total planet. The maximum normalized moment of inertia also decreased from 0.353 to 0.344. The controls on interior structure change as well. For a given core radius, the molten material parameters indicate less sulfur in the core than substituting the solid parameters would suggest (Figure 4).

4.3. Moment of Inertia

[39] All of the modeled cases produced normalized moments of inertia of 0.319–0.353, consistent with previous work [*Harder and Schubert*, 2001]. *Harder and Schubert* [2001] found normalized moments of inertia up to 0.380

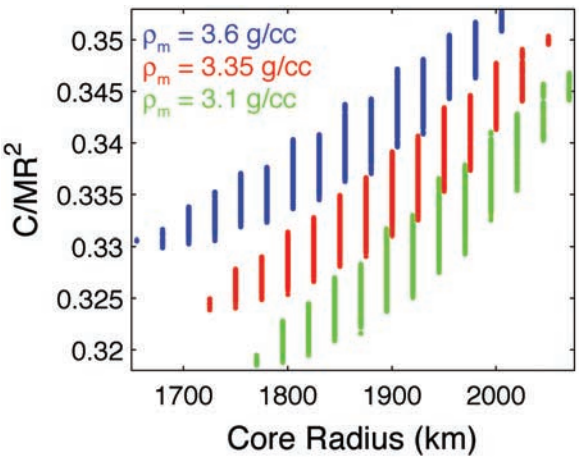

Figure 2. The correlation between the core radius and normalized moment of inertia changes with the mantle density (indicated by the color of the data points). This dependence introduces considerable scatter in the correlation and the normalized moment of inertia does not constrain the total core radius well. The core radius (x axis) is offset by ±5 km for clarity.

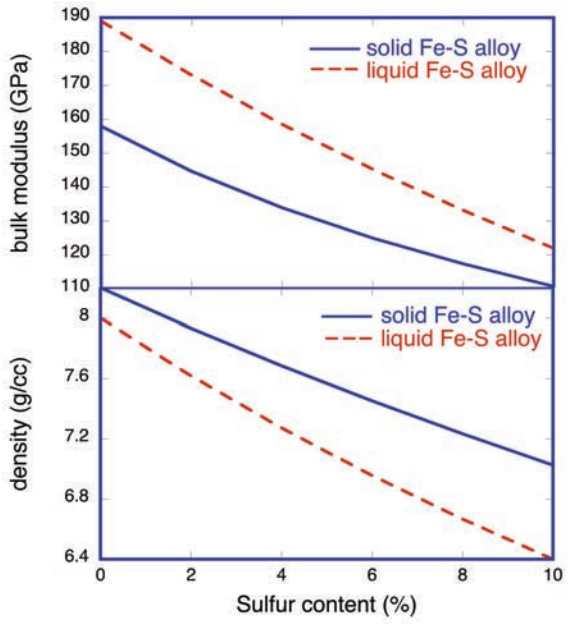

Figure 3. The density and bulk modulus of Fe and Fe alloys as a function of sulfur content. The liquid is less dense and less compressible than the solid. The material properties of a given bulk core sulfur content vary depending on the distribution of mass and sulfur between the molten outer core and the solid inner core, due to variations in the material properties of molten and solid iron alloys illustrated here.

but note that normalized moments of inertia above 0.350 require Fe:S atomic ratios lower than the cosmic abundance (Fe:S = 2.88).

[40] The normalized moment of inertia is most sensitive to the mass, radius and sulfur content of the core. Not surprisingly, larger, more massive, and more sulfur-rich cores have larger normalized moments of inertia. The MESSENGER mission will measure the moment of inertia of Mercury within ±0.34% (D. E. Smith, personal communication, 2007). Even with the small error, there is significant uncertainty in the interpretation of the normalized moment of inertia given the number of poorly constrained parameters for Mercury (for example, see Figure 2). We use our model to illustrate this point for the mantle parameters, crust parameters and self-compression considerations.

[41] The mantle density controls the normalized moment of inertia, but to a lesser degree than the core parameters. High mantle densities increase the mass in the mantle, and the mass of the core must decrease to satisfy the total mass constraint. Therefore higher-density mantles tend to correlate with smaller, less sulfur-rich cores and produce higher normalized moments of inertia, though there is significant overlap (Figure 2).

[42] Thus far we have neglected the crust. Uncertainties in the thickness and density of Mercury's crust significantly contribute to the uncertainty in the correlation of the normalized moment of inertia to the size of the core. For crusts 0–200 km deep with densities 2.8–3.2 g cm^{-3}, uncertainties in size and density of the crust introduce variations in the normalized moments of inertia for a given core radius up to 0.005, or 10–20% to the total range of normalized moments of inertia for a given core radius and about five times the error bars predicted for the normalized moment of inertia from MESSENGER.

[43] Self-compression within a single homogeneous layer does affect the normalized moment of inertia. Simple constant density models can be useful for understanding qualitative relationships among variables but the moment of inertia values calculated by such models should not be compared to observed measurements. In a constant density model, a homogeneous core has a normalized moment of inertia of 0.4. The single layer cores in our results have core normalized moments of inertia between 0.388 and 0.395. For the density and pressures of Mercury's core, constant density models introduce normalized moment of inertia errors of 0.5–1.5%, approximately 10% of the full range of plausible values.

[44] Given the uncertainties in the mantle, core, and thermal parameters reflected in the input parameters (reflected in Table 3) even the precise measurement of the normalized moment of inertia by MESSENGER will not closely limit the interior structure of Mercury without additional constraints. Because Mercury's mantle is decoupled from the core, as shown by recent Earth based measurements of the amplitude of the forced physical libration of Mercury [*Margot et al.*, 2007] the ratio of the moment of inertia of the mantle to that of the whole planet (C_m/C) can be determined via knowledge of Mercury's obliquity, forced physical libration amplitude, and low degree and order gravity field coefficients C_{20} and C_{22} [*Peale et al.*, 2002].

[45] Together, C/MR^2 and C_m/C tightly constrain the core radius and mass. Given knowledge of C/MR^2 within ±0.34% and C_m/C within ±6% [*Margot et al.*, 2007], the

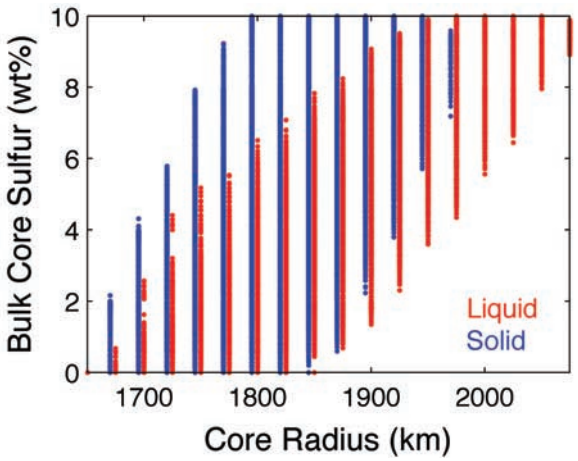

Figure 4. The correlation between core radius and core bulk sulfur (shown in Figure 1) changes if the material properties of liquids are assumed to be similar to those of solids. The red points are those that use the new experimental values of liquid iron alloys for the outer core and the blue points are the results of the same model if the material properties of liquids and solids are assumed to be comparable (as in previous studies) and solid parameters are used for both the outer and the inner core. Using newly measured molten core properties the plausible sulfur abundance for a given core radius is lower.

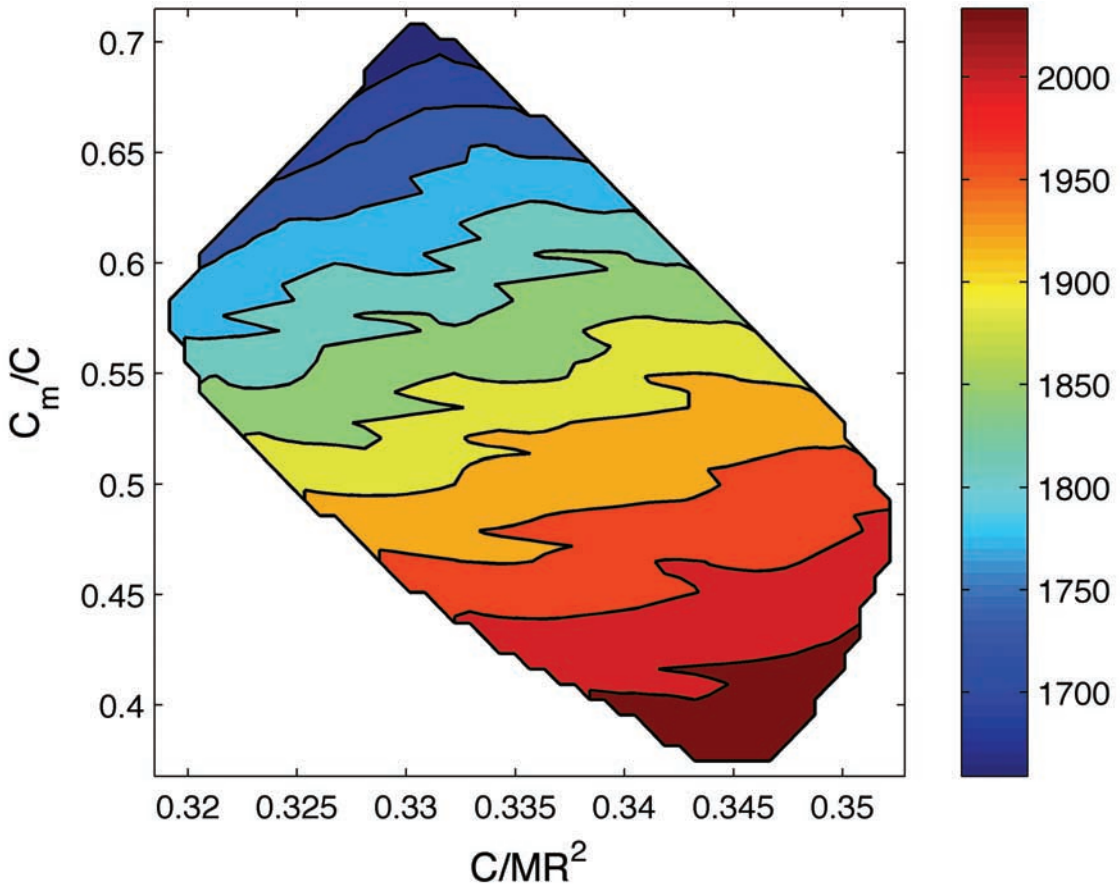

Figure 5. The moment of inertia parameters, C/MR^2 and C_m/C tightly constrain the total core radius (indicated by the color of the contours).

radius of the core is constrained within 100 km (Figure 5) and the core mass fraction is constrained within 5% of the total planet mass. Even under C/MR^2 and C_m/C constraints, in some cases the bulk core sulfur content varies by 8 wt% and the radius of the inner core and the mass fraction of molten core materials are essentially unconstrained. The reader is cautioned that these constraints are affected by the step size used in the grid search and should be taken as rough estimates on the knowledge of each parameter. *Hauck et al.* [2007] give a good description of uncertainty estimates from grid searches versus Monte Carlo methods. We find that the details of the distribution of sulfur between molten outer core and solid inner core with varying relative masses introduces more uncertainty in the bulk sulfur content than was represented by previous studies of single layer cores.

[46] If the mass and radius of the core can be constrained from knowledge of C/MR^2 and C_m/C, the normalized moment of inertia of the core, $C_c/M_cR_c^2$ can be estimated (note that $C = C_m + C_c$). It has been suggested that this value can be used to determine the radius of the inner core [*Spohn et al.*, 2001]. The relative densities of the inner and outer cores must be known in order to use $C_c/M_cR_c^2$ to constrain the inner core radius. In a few cases (low S in inner and outer core, low ΔT at both the CMB and ICB), the density change at the inner core boundary may be very small leading to $C_c/M_cR_c^2$ values closer to 0.4 than highly compressible single layer cores. Uncertainties in the composition of the inner and outer core, in thermal gradients across the CMB and ICB, and in the thermal expansion and compressibility core materials, make the interpretation of the core normalized moment of inertia ambiguous.

[47] Additional high-pressure experiments on molten and solid iron alloys could shed light on this problem. More experimental data on the partitioning of sulfur between liquid and solid phases at the pressures relevant to Mercury's core are needed in order to constrain the ratio of the core densities and make a better estimate of the inner core radius. Laboratory high-pressure experiments will play an important role in fully understanding the geophysical measurements anticipated by spacecraft missions.

4.4. Decompressed Density

[48] New ideas about the formation of the Solar System and planets, along with advances in high-pressure experiments have added much new knowledge since decompressed density estimates were first published. In this study, we estimate the decompressed density of Mercury, documenting the methodology and assumptions and provide an analysis of the sensitivity to the input parameters. Finally we present implications for scientific interpretation of the decompressed densities of the terrestrial planets.

[49] In order for the decompressed density to be used as a mass-insensitive measure of the bulk composition of any

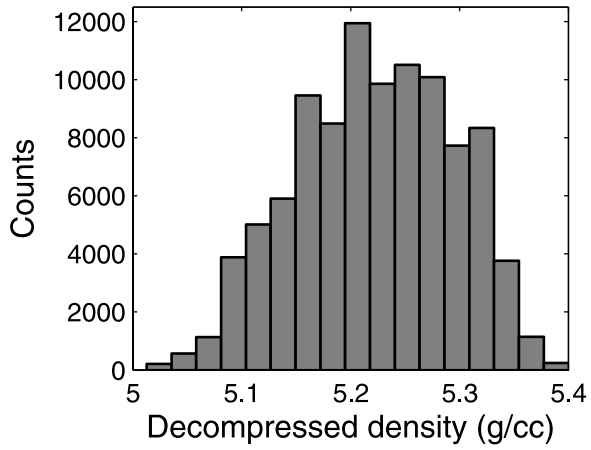

Figure 6. Decompressed density values for over 41,800 cases within 0.1% of Mercury's mass. The mean value is 5.23 ± 0.07 (1σ) g cm^{-3}.

size planet, complete correction for high-temperature and high-pressure phases is necessary. Thermal expansion effects in the interior of small bodies compete with compression effects of pressure and reduce the overall compression. For small bodies [*BVSP*, 1981] or bodies with a large molten component, the decompressed density may be larger than the average density. This is an effect of both cooling and decompressing the material to arrive at a decompressed density estimate. The appropriate standard pressure and temperature (STP) density must be selected for calculating the decompressed density. The zero-pressure density of high-pressure phases is often reported at high temperature. These densities must be corrected to low temperature to compare different sized bodies. Finally the occurrence of high-pressure phase changes and molten materials are influenced by the total mass of the body. Therefore the density of the phases that occur at STP, not the zero-pressure density of high-pressure phases, should be used for the calculation of decompressed density.

[50] Our systematic grid search indicates the decompressed density of Mercury lies between 5.06 and 5.34 g cm^{-3} with the mean decompressed density being 5.2 ± 0.05 (1σ) g cm^{-3} (Figure 6). Models with entirely solid cores have decompressed densities between 5.0 and 5.1 g cm^{-3} (mean 5.1 g/cm^3 ± 0.03 (1σ)), well below the previously published value of 5.3 g cm^{-3}.

[51] The decompressed density is correlated with the size, mass and sulfur content of the liquid outer core (Figure 7). This correlation is due to the relationship between the phase-specific density and the STP density of core materials. For solid Fe-S alloys and liquid Fe-S alloys with less than ~2 wt% S, the STP density of any Fe-S composition is lower than the zero-pressure density for that phase. At higher sulfur contents, molten Fe-S alloys are less dense than the STP phase (Figure 8). Thus molten Fe-S materials with greater than ~2 wt% S require a positive correction for compression and result in higher decompressed densities. If we calculate the decompressed density using the STP density of the phase that occurs in the planet (e.g., γ fcc Fe or molten Fe-S alloy), then the relationship between core size, mass and sulfur content reverses and weakens and larger, more massive, sulfur-rich cores have lower decompressed densities because adding sulfur to the core makes it more compressible and the resulting correction to the average density is larger. In all cases, the decompressed density is sensitive to the thermal parameters (Figure 7b). Steeper gradients across the thermal boundary layers result in greater thermal expansion, which counters compression due to pressure and increases the decompressed density.

[52] Knowledge of the decompressed density of Mercury is most useful when compared to that of the other terrestrial planets. However, meaningful comparisons are problematic because the decompressed density calculations for the other terrestrial planets are not well documented. Additionally, the definition of the decompressed density varies among published estimates. For example, published decompressed densities for the Earth cluster around 4.0–4.1 g cm^{-3} and 4.4 g cm^{-3} [*Lewis*, 1972, 1988; *Urey*, 1951; *Wasson*, 1988].

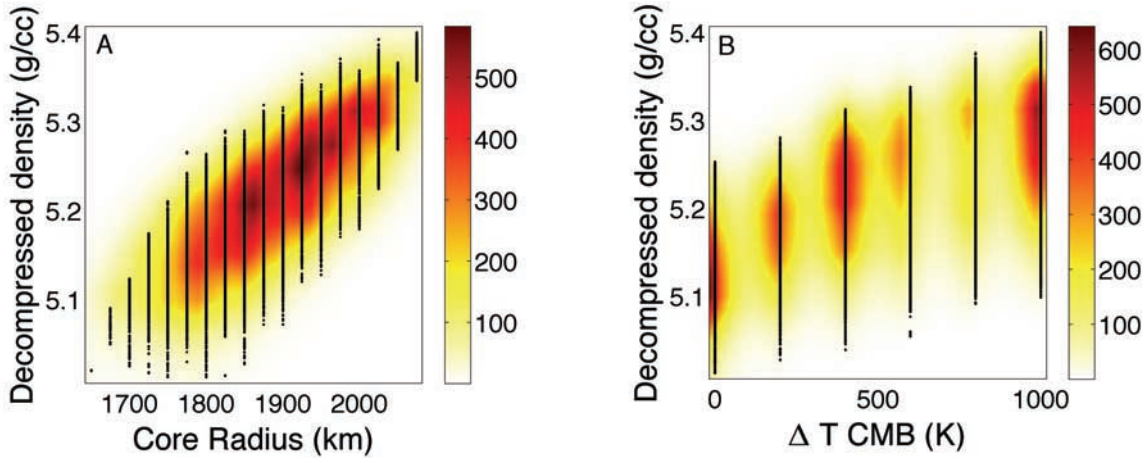

Figure 7. The decompressed density is sensitive to the size, mass and sulfur content of the core and the steepness of the temperature gradient across thermal boundary layers. Two representative examples are shown here, (a) core radius and (b) temperature change at the CMB. As with the other correlations presented above, there is significant spread in the data due to variations in other core, mantle and thermal parameters.

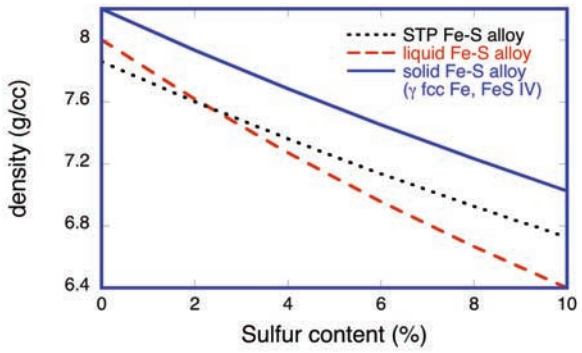

Figure 8. The density as a function of sulfur content (wt. %) for solid mixtures of γ fcc Fe and FeS IV, molten Fe-S, and mixtures of the STP phases: α bcc Fe and FeS III. For solid alloys and molten alloys with <2 wt% S the STP phase is less dense than the density of the high-pressure/high-temperature phase extrapolated to zero pressure, 300 K. At S contents >2 wt% the STP phase is more dense than the phase that occurs in the planet. This influences the sensitivity of the decompressed density to the phase and sulfur content of the core.

In applying our methods to Earth, we have found that this duality simply reflects different interpretations of the definition of decompressed density. If the decompressed density is to be used as a mass-independent parameter to compare the bulk composition of planetary bodies, then the density must be corrected for all mass-dependent effects, including self-compression, high-pressure phases, and melting in the interior.

4.5. Effect of Uncertain Input Parameters

[53] Given uncertainty in the light-alloying element in Mercury's core, it is possible that the inner core contains no light alloying element. We examined the effect of allowing the amount of light alloying element in the inner core to vary by comparing our results presented above (Sic = 0–4 wt%) with results restricting the composition of the inner core to Sic = 0 wt%. We find that allowing the light alloying element composition of the inner core to vary has little effect on the range of plausible interior structures. The maximum radius of the inner core decreased by 50 km (from 1850 km to 1800 km), or two times the step size. However, uncertainty in the inner core composition becomes important when interpreting the moment of inertia values, C_m/C and C/MR^2. The predicted recovery of Mercury's interior properties from moment of inertia measurements does not change if we consider the inner core known (0% light alloying element) with the exception of the total core sulfur content. For Sic 0–4 wt% and the moment of inertia parameters known within predicted errors, the sulfur content of the core may vary by 6.5 wt%, if we restrict Sic to 0 wt% then the sulfur content of the inner core may vary by 5.2 wt%. Allowing the light alloying element composition of the inner core to vary is most important when interpreting the anticipated core normalized moment of inertia. Anticipated spacecraft measurements will allow an estimate of the normalized moment of inertia of the core (since $C = C_m + C_c$ and knowledge of C/MR^2 and C_m/C together will constrain the mass and radius of the core). In that case the composition of the inner and outer cores and the size of the inner core are unknown. If one assumes the composition of the inner core is known, one of three variables is removed and narrows the possible core structures and compositions that match anticipated observations. We include uncertainty in the inner core composition to reflect the uncertainty in the light alloying element present in Mercury's core, variations in the eutectic behavior of different candidate light alloying elements and uncertainty in the crystallization mechanisms in Mercury's core.

[54] The thermal parameters have a minor effect on the modeled interior structure and composition of Mercury (Table 6). At a given core radius, changes between the extreme thermal parameters can expand the plausible sulfur content by approximately ±0.5%. The thermal parameters do not change the core radius-moment of inertia correlation, but restricting the results to the lowest ΔT values can decrease the core radius range by ~50 km, resulting in a small decrease in the maximum normalized moment of inertia. As mentioned above, the decompressed density is most affected by uncertainty in Mercury's thermal profile.

5. Discussion

[55] New high-pressure experiments on the properties of molten Fe-S alloys [*Balog et al.*, 2003; *Sanloup et al.*, 2000] together with the discovery of a partially or fully molten Mercurian core [*Margot et al.*, 2007], provide an opportunity

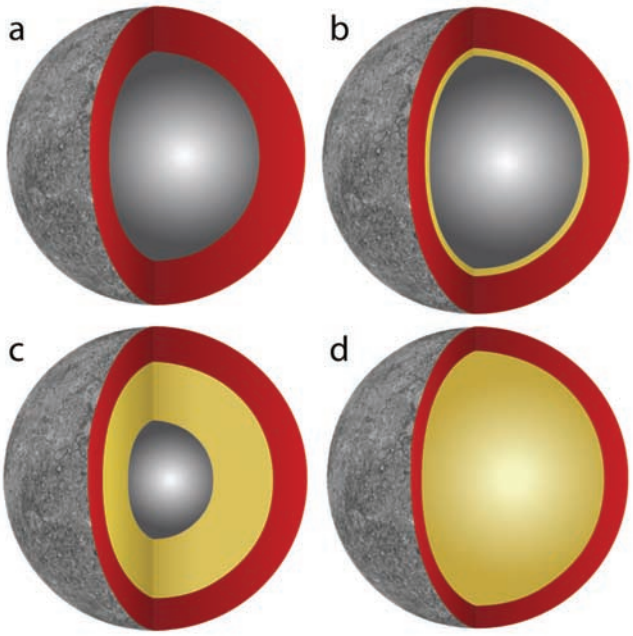

Figure 9. Four possible density structures of Mercury demonstrating the wide range of plausible compositions and interior structures. (a) solid Fe core, (b) solid Fe inner core with thin (100 km) molten Fe 1% S outer core, (c) layered core, radius of the inner core is one half the radius of the total core, the outer core is Fe 4 wt% S outer core and the inner core is pure Fe and (d) entirely molten Fe 10 wt% S core. The input parameters and the resulting moment of inertia parameters, decompressed densities and core mass fractions are listed in Table 7.

for a fresh look at Mercury's interior. We have incorporated the elastic properties of molten core materials, layered cores and a geochemically plausible range of core sulfur contents into a new model of Mercury's interior. Our results show the wide range of plausible structures and compositions of Mercury. We have demonstrated that models with layered and molten cores are required to accurately assess the origin and evolution of Mercury and to give context to the moment of inertia and magnetic field measurements that will be made in the near future by spacecraft. Our model results will help achieve a confident but possibly nonunique interpretation of Mercury's density structure.

5.1. Formation Hypotheses Implications

[56] Given our input parameters and assumptions, Mercury's core mass fraction is significantly larger than the other terrestrial planets and has a broad range of plausible values (53–78% of the total planet mass). This broad range of plausible core mass fractions has several implications for the hypotheses of iron enrichment of Mercury (equilibrium condensation, silicate vaporization, giant impact and aerodynamic fractionation). First, models attempting to explain the high density of Mercury have assumed a solid iron core with no light alloying element and have not included the full range of plausible core sizes and compositions [*Benz et al.*, 1988; *Cameron*, 1985; *Fegley and Cameron*, 1987]. Additionally, these models have not addressed the core size or composition expected from the chemical and physical processes invoked to explain the iron enrichment. Finally, previous workers have focused on the composition of Mercury's silicate component to distinguish between iron enrichment hypotheses [e.g., *Taylor and Scott*, 2003]. The composition, size and phase of the core are also constraints on the iron enrichment of Mercury and should be considered in more detail. In light of the recently discovered molten core of Mercury and in anticipation of new complementary spacecraft geophysical observations, core characteristics should be incorporated into evaluations of the viability of iron enrichment hypotheses.

[57] Formation hypotheses that require Mercury to accrete with a more familiar (i.e., chondritic) metal mass fraction (sometimes presented as the metal to silicate ratio) and subsequently lose silicate material by vaporization or giant impact have not typically addressed the possibility of a light alloying element in the core [*Benz et al.*, 1988; *Cameron*, 1985; *Fegley and Cameron*, 1987]. Silicate loss hypotheses typically assume Mercury's core is ~60% of the total mass and extrapolate back to a proto-Mercury with a lower metal content. Depending on the amount of light alloying element or elements present and the extent of the molten layer, the current metal mass fraction can be much greater than the typical value of 60% and more silicate loss is required to explain the assumed proto-Mercury metal mass fraction. It is unclear if existing iron enrichment hypotheses can account for the increased silicate loss required for larger cores. If they can account for additional silicate loss, how do the formation parameters and predicted silicate compositions change? Furthermore, it is unclear how the silicate loss processes would affect the composition of the core, particularly moderately volatile, light alloying elements. Additional modeling of iron enrichment hypotheses considering a variety of plausible interior structures to make testable predictions (using both the silicate and metal components) will aid in interpretation of spacecraft data to test hypotheses of iron enrichment.

5.2. Importance of Molten Material Properties

[58] Understanding the composition and interior structure of Mercury requires an understanding of the density of candidate materials as a function of temperature and pressure. In addition to recent Earth-based radar observations and anticipated spacecraft observations, additional high-pressure experiments on the elastic properties of plausible core materials are necessary to accurately determine the bulk composition of Mercury and the state of its interior. Anticipated accurate measurements of C/MR^2, C_m/C and $C_c/M_cR_c^2$ require knowledge of the density of plausible core materials under relevant pressure and temperature conditions. In particular, few measurements of the thermoelastic properties of Fe-S liquids at relevant temperatures and pressures exist. Even less experimental data is available for other light alloying elements. Without these data we cannot definitively identify the light alloying element or elements that have lowered the melting temperature of Mercury's core to allow a molten layer to be present. Additional knowledge of the melting behavior of Fe-S alloys, as well as other candidate light elements, is necessary to interpret anticipated $C_c/M_cR_c^2$ values.

[59] We have demonstrated that the material properties of molten iron alloys are sufficiently different from that of solid iron alloys to change the results of any interior model of Mercury. The incorporation of molten iron and iron alloy equations of state to the model increases the plausible core size by over 100 km. Perhaps more important for interpreting future spacecraft observations, the amount of sulfur plausible for a given core radius decreases when molten material properties are used. Additionally, modeling with layered cores increases the number of variables and the complexity of the model, thus introducing more uncertainty in relationships between compositional and structural parameters or between observations and inferred properties. For example, in a single layer model the core radius and core sulfur content are tightly constrained by C/MR^2 for a given mantle density [e.g., *Harder and Schubert*, 2001]. We have shown that for a layered core, the range of plausible core compositions and sizes varies by a factor of two more than the single layer case because there are more degrees of freedom. The predictive capabilities of geophysical parameters that may be measured by spacecraft are strongly affected by the presence of a layered core.

5.3. Future Spacecraft Missions

[60] The MESSENGER spacecraft is en route to Mercury with an instrument suite designed to address the composition and interior structure of Mercury [*Solomon et al.*, 2001] and the ESA BepiColombo mission to Mercury is under development [*Spohn et al.*, 2001]. These missions will constrain the composition of the silicate portion of Mercury and accurately measure C/MR^2 and C_m/C and thus better constrain the density structure of Mercury and help distinguish between the structures presented here. Interpretation of MESSENGER observations with previously published models will result in oversimplified or even incorrect

conclusions. Because our model incorporates layered cores and molten core materials our results are better suited to support analysis of anticipated spacecraft geophysical observations.

6. Conclusions

[61] The recent discovery of a partially or fully molten Mercurian core [*Margot et al.*, 2007] and newly available experimental results on the material properties of molten Fe alloys provide an opportunity for more accurate models of Mercury's interior. We have incorporated molten core materials, layered cores and cosmochemically plausible core compositions into new models of Mercury's density structure.

[62] We find that Mercury's interior structure and composition can vary widely. Depending on the amount of light alloying element (0–10 wt%), the core can be between 1675 and 2075 km in radius and 53–78% of the total planet mass. The canonical value of the decompressed density of Mercury, 5.3 g cm^{-3} is possible, but we find a mean value of 5.2 ± 0.07 (σ) g cm^{-3} and a range of plausible values from 5.0 to 5.4 g cm^{-3}. The mantle and thermal parameters have a second-order effect on the modeled interior structures and compositions of Mercury's core.

[63] The existing hypotheses of Mercury's iron enrichment are unsatisfying. Equilibrium condensation seems unlikely on the basis of dynamical accretion arguments and by the presence of a partially or fully molten core, implying a volatile light alloying element [*Margot et al.*, 2007]. The silicate loss hypotheses (giant impact and vaporization) assume a solid iron core of approximately 60% of the mass of the planet. It is unclear how these hypotheses might change if Mercury is more enriched in metal. Furthermore, none of these hypotheses have explicitly addressed potential changes to core chemistry in the process of silicate loss. Explicit modeling of the fate of moderately volatile light alloying elements in the core during silicate vaporization or giant impact would provide an important test of each hypothesis.

[64] Incorporation of layered cores and molten core material properties changes models of Mercury's density structure, extending the range of plausible core sizes and changing relationships between core composition and size. In light of new measurements showing Mercury's core is partially or fully molten future models of Mercury's interior need to include the density and elastic properties of molten core materials.

[65] We have demonstrated the importance of considering molten and layered cores on the accurate interpretation of anticipated geophysical measurements from spacecraft missions (i.e., C/MR^2 and C_m/C). C/MR^2 alone does not constrain the size of the core if Mercury has a layered core. The combination of C/MR^2 and C_m/C will tightly constrain the core size but not necessarily constrain the core composition or the extent of the molten portion of the core. The core normalized moment of inertia ($C_c/M_cR_c^2$) will not constrain the extent of the molten core without knowledge of the relative densities of the inner and outer core (ρ_{oc}/ρ_{ic}). The models presented here can be used to interpret the moment of inertia values that will be calculated from Earth-based radar and future spacecraft tracking measurements.

[66] **Acknowledgments.** The authors would like to thank Allen McNamara, Teresa Lassak, and Eric Mittelstaedt for helpful discussions and Sue Selkirk for her assistance with graphics. Comments from Stan Peale, Steve Hauck, and an anonymous reviewer helped clarify the manuscript. This work was supported by NASA's Planetary Geology and Geophysics program.

References

Aharonson, O., M. T. Zuber, and S. C. Solomon (2004), Crustal remanence in an internally magnetized non-uniform shell: A possible source for Mercury's magnetic field?, *Earth Planet. Sci. Lett.*, *218*, 261–268, doi:10.1016/S0012-821X(03)00682-4.

Ahrens, T. J., K. G. Holland, and G. Q. Chen (2002), Phase diagram of iron, revised-core temperatures, *Geophys. Res. Lett.*, *29*(7), 1150, doi:10.1029/2001GL014350.

Anderson, O. L., and D. G. Isaak (2002), Another look at the core density deficit of Earth's outer core, *Phys. Earth Planet Inter.*, *131*, 19–27, doi:10.1016/S0031-9201(02)00017-1.

Anderson, W. W., and T. J. Ahrens (1994), An equation of state for liquid iron and implications for the Earth's core, *J. Geophys. Res.*, *99*, 4273–4284, doi:10.1029/93JB03158.

Badro, J., G. Fiquet, F. Guyot, E. Gregoryanz, F. Occelli, D. Antonangeli, and M. d'Astuto (2007), Effect of light elements on the sound velocities in solid iron: Implications for the composition of Earth's core, *Earth Planet. Sci. Lett.*, *254*, 233–238, doi:10.1016/j.epsl.2006.11.025.

Balog, P. S., R. A. Secco, D. C. Rubie, and D. J. Frost (2003), Equation of state of liquid Fe-10 wt % S: Implications for the metallic cores of planetary bodies, *J. Geophys. Res.*, *108*(B2), 2124, doi:10.1029/2001JB001646.

Basaltic Volcanism Study Project (BVSP) (1981), *Basaltic Volcanism on Terrestrial Planets*, 1286 pp., Pergamon Press, New York.

Benz, W., W. L. Slattery, and A. G. W. Cameron (1988), Collisional stripping of Mercury's mantle, *Icarus*, *74*, 516–528, doi:10.1016/0019-1035(88)90118-2.

Bina, C. R., and G. R. Helffrich (1992), Calculation of elastic properties from thermodynamic equation of state principles, *Annu. Rev. Earth Planet. Sci.*, *20*, 527–552, doi:10.1146/annurev.ea.20.050192.002523.

Blewett, D. T., P. G. Lucey, B. R. Hawke, G. G. Ling, and M. S. Robinson (1997), A comparison of Mercurian reflectance and spectral quantities with those of the Moon, *Icarus*, *129*, 217–231, doi:10.1006/icar.1997.5785.

Boehler, R., J. M. Besson, M. Nicol, M. Nielsen, J. P. Itie, G. Weill, S. Johnson, and F. Grey (1989), X-ray diffraction of gamma-Fe at high temperatures and pressures, *J. Appl. Phys.*, *65*, 1795–1797.

Boehler, R., N. Vonbargen, and A. Chopelas (1990), Melting, thermal-expansion, and phase-transitions of iron at high pressures, *J. Geophys. Res.*, *95*, 21,731–21,736, doi:10.1029/JB095iB13p21731.

Cameron, A. G. W. (1985), The partial volatilization of Mercury, *Icarus*, *64*, 285–294, doi:10.1016/0019-1035(85)90091-0.

Chen, B., L. L. Gao, K. Funakoshi, and J. Li (2007), Thermal expansion of iron-rich alloys and implications for the Earth's core, *Proc. Natl. Acad. Sci. U. S. A.*, *104*(22), 9162–9167, doi:10.1073/pnas.0610474104.

Christensen, U. R. (2006), A deep dynamo generating Mercury's magnetic field, *Nature*, *444*, 1056–1058, doi:10.1038/nature05342.

Davies, G., and A. Dziewonski (1975), Homogeneity and constitution of the Earth's lower mantle and outer core, *Phys. Earth Inter.*, *10*, 336–343.

Fegley, B., Jr., and A. G. W. Cameron (1987), A vaporization model for iron/silicate fractionation in the Mercury protoplanet, *Earth Planet. Sci. Lett.*, *82*, 207–222, doi:10.1016/0012-821X(87)90196-8.

Fei, Y., C. T. Prewitt, H. K. Mao, and C. M. Bertka (1995), Structure and density of FeS at high pressure and high temperature and the internal structure of Mars, *Science*, *268*, 1892–1894, doi:10.1126/science.268.5219.1892.

Fei, Y., J. Li, C. M. Bertka, and C. T. Prewitt (2000), Structure type and bulk modulus of Fe_3S, a new iron-sulfur compound, *Am. Mineral.*, *85*, 1830–1833.

Folkner, W. M., C. F. Yoder, D. N. Yuan, E. M. Standish, and R. A. Preston (1997), Interior structure and seasonal mass redistribution of Mars from radio tracking of Mars Pathfinder, *Science*, *278*, 1749–1752, doi:10.1126/science.278.5344.1749.

Giampieri, G., and A. Balogh (2002), Mercury's thermoelectric dynamo model revisited, *Planet. Space Sci.*, *50*, 757–762, doi:10.1016/S0032-0633(02)00020-X.

Goettel, K. A. (1988), Present bounds on the bulk composition of Mercury: Implications for planetary formation processes, in *Mercury*, edited by F. Vilas et al., pp. 613–621, Univ. of Ariz. Press, Tucson.

Harder, H. H., and G. Schubert (2001), Sulfur in Mercury's core?, *Icarus*, *115*, 118–122.

Hauck, S. A., A. J. Dombard, R. J. Phillips, and S. C. Solomon (2004), Internal and tectonic evolution of Mercury, *Earth Planet. Sci. Lett.*, *222*, 713–728, doi:10.1016/j.epsl.2004.03.037.

Hauck, S. A., S. C. Solomon, and D. A. Smith (2007), Predicted recovery of Mercury's internal structure by MESSENGER, *Geophys. Res. Lett.*, *34*, L18201, doi:10.1029/2007GL030793.

Heimpel, M. H., J. M. Aurnou, F. M. Al-Shamali, and N. G. Perez (2005), A numerical study of dynamo action as a function of spherical shell geometry, *Earth Planet. Sci. Lett.*, *236*, 542–557, doi:10.1016/j.epsl.2005.04.032.

Hixson, R. S., M. A. Winkler, and M. L. Hodgdon (1990), Sound speed and thermophysical properties of liquid-iron and nickel, *Phys. Rev. B*, *42*, 6485–6491, doi:10.1103/PhysRevB.42.6485.

Knittle, E. (1995), Static compression measurements of equations of state, in *Mineral Physics and Crystallography: A Handbook of Physical Constants*, edited by T. J. Ahrens, pp. 98–142, AGU, Washington, D. C.

Kortenkamp, S. J., E. Kokubo, and S. J. Weidenschilling (2000), Formation of planetary embryos, in *Origin of the Earth and Moon*, edited by R. M. Canup and K. Righter, pp. 85–100, Univ. of Ariz. Press, Tucson.

Kozlovskaya, (1969), On internal constitution and chemical composition of Mercury, *Astrophys. Lett.*, *4*, 1–4.

Lewis, J. S. (1972), Metal-silicate fractionation in Solar System, *Earth Planet. Sci. Lett.*, *15*, 286–290, doi:10.1016/0012-821X(72)90174-4.

Lewis, J. S. (1988), Origin and composition of Mercury, in *Mercury*, edited by F. Vilas et al., pp. 651–666, Univ. of Ariz. Press, Tucson.

Li, J., and Y. Fei (2003), Experimental constraints on core composition, in *Treatise on Geochemistry*, vol. 2, *The Mantle and Core*, edited by R. W. Carlson, pp. 521–546, Elsevier, Amsterdam.

Mao, H. K., Y. Wu, L. C. Chen, J. F. Shu, and A. P. Jephcoat (1990), Static compression of iron to 300 GPa and $Fe_{0.8}Ni_{0.2}$ Alloy to 260 GPa: Implications for composition of the core, *J. Geophys. Res.*, *95*, 21,737–21,742, doi:10.1029/JB095iB13p21737.

Margot, J. L., S. J. Peale, R. F. Jurgens, M. A. Slade, and I. V. Holin (2007), Large longitude libration of Mercury reveals a molten core, *Science*, *316*, 710–714, doi:10.1126/science.1140514.

McCord, T. B., and R. N. Clark (1979), The Mercury soil: Presence of Fe^{2+}, *J. Geophys. Res.*, *84*, 7664–7668.

Nasch, P. M., and S. G. Steinemann (1995), Density and thermal expansion of molten manganese, iron, nickel, copper, aluminum and tin by means of the gamma-ray attenuation technique, *Phys. Chem. Liquids*, *29*, 43–58, doi:10.1080/00319109508030263.

Ness, N. F., K. W. Behannon, R. P. Lepping, Y. C. Whang, and K. H. Schatten (1974), Magnetic field observations near Mercury: Preliminary results from Mariner 10, *Science*, *185*, 151–160, doi:10.1126/science.185.4146.151.

Peale, S. J. (1976), Does Mercury have a molten core, *Nature*, *262*, 765–766, doi:10.1038/262765a0.

Peale, S. J., R. J. Phillips, S. C. Solomon, D. E. Smith, and M. T. Zuber (2002), A procedure for determining the nature of Mercury's core, *Meteorit. Planet. Sci.*, *37*, 1269–1283.

Potter, A., and T. Morgan (1985), Discovery of sodium in the atmosphere of Mercury, *Science*, *229*, 651–653, doi:10.1126/science.229.4714.651.

Potter, A., and T. Morgan (1986), Potassium in the atmosphere of Mercury, *Icarus*, *67*, 336–340, doi:10.1016/0019-1035(86)90113-2.

Redmond, H. L., and S. D. King (2007), Does mantle convection currently exist on Mercury?, *Phys. Earth Planet. Inter.*, *164*(3–4), 221–231, doi:10.1016/j.pepi.2007.07.004.

Reynolds, R. T., and A. L. Summers (1969), Calculations on the composition of the terrestrial planets, *J. Geophys. Res.*, *74*, 2494–2511, doi:10.1029/JB074i010p02494.

Robinson, M. S., and P. G. Lucey (1997), Recalibrated Mariner 10 color mosaics: Implications for Mercurian volcanism, *Science*, *275*, 197–200, doi:10.1126/science.275.5297.197.

Robinson, M. S., and G. J. Taylor (2001), Ferrous oxide in Mercury's crust and mantle, *Meteorit. Planet. Sci.*, *36*, 841–847.

Sanloup, C., F. Guyot, P. Gillet, G. Fiquet, M. Mezouar, and I. Martinez (2000), Density measurements of liquid Fe-S alloys at high-pressure, *Geophys. Res. Lett.*, *27*, 811–814, doi:10.1029/1999GL008431.

Schubert, G., M. N. Ross, D. J. Stevenson, and T. Spohn (1988), Mercury's thermal history and the generation of its magnetic field, in *Mercury*, edited by F. Vilas et al., pp. 429–460, Univ. of Ariz. Press, Tucson.

Siegfried, R. W., and S. C. Solomon (1974), Mercury: Internal structure and thermal evolution, *Icarus*, *23*, 192–205, doi:10.1016/0019-1035(74)90005-0.

Solomon, S. C. (1976), Some aspects of core formation in Mercury, *Icarus*, *28*, 509–521, doi:10.1016/0019-1035(76)90124-X.

Solomon, S. C., et al. (2001), The MESSENGER mission to Mercury: Scientific objectives and implementation, *Planet. Space Sci.*, *49*, 1445–1465, doi:10.1016/S0032-0633(01)00085-X.

Spohn, T., F. Sohl, K. Wieczerkowski, and V. Conzelmann (2001), The interior structure of Mercury: What we know, what we expect from BepiColombo, *Planet. Space Sci.*, *49*, 1561–1570, doi:10.1016/S0032-0633(01)00093-9.

Srnka, L. J. (1976), Magnetic dipole moment of a spherical shell with TRM acquired in a field of internal origin, *Phys. Earth Planet. Inter.*, *11*, 184–190, doi:10.1016/0031-9201(76)90062-5.

Stanley, S., J. Bloxham, W. E. Hutchison, and M. T. Zuber (2005), Thin shell dynamo models consistent with Mercury's weak observed magnetic field, *Earth Planet. Sci. Lett.*, *234*, 27–38, doi:10.1016/j.epsl.2005.02.040.

Stephenson, A. (1976), Crustal remanence and magnetic-moment of Mercury, *Earth Planet. Sci. Lett.*, *28*, 454–458, doi:10.1016/0012-821X(76)90206-5.

Stevenson, D. J. (2003), Planetary magnetic fields, *Earth Planet. Sci. Lett.*, *208*, 1–11, doi:10.1016/S0012-821X(02)01126-3.

Stevenson, D. J., T. Spohn, and G. Schubert (1983), Magnetism and thermal evolution of the terrestrial planets, *Icarus*, *54*, 466–489, doi:10.1016/0019-1035(83)90241-5.

Taylor, G. J., and E. R. D. Scott (2003), Mercury, in *Treatise on Geochemistry: Meteorites, Comets and Planets*, edited by A. M. Davis, pp. 477–485, Elsevier, Amsterdam.

Turcotte, G., and G. Schubert (2002), *Geodynamics*, 456 pp., Cambridge Univ. Press, Cambridge, UK.

Urakawa, S., et al. (2004), Phase relationships and equations of state for FeS at high pressures and temperatures and implications for the internal structure of Mars, *Phys. Earth Planet. Inter.*, *143–144*, 469–479, doi:10.1016/j.pepi.2003.12.015.

Urey, H. C. (1951), The origin and development of the earth and other terrestrial planets, *Geochim. Cosmochim. Acta*, *1*, 209–277, doi:10.1016/0016-7037(51)90001-4.

Van Hoolst, T., and C. Jacobs (2003), Mercury's tides and interior structure, *J. Geophys. Res.*, *108*(E11), 5121, doi:10.1029/2003JE002126.

Vilas, F. (1988), Surface composition of Mercury from reflectance spectrophotometry, in *Mercury*, edited by F. Vilas et al., pp. 59–76, Univ. of Ariz. Press, Tucson.

Wasson, J. T. (1988), The building stones of the planets, in *Mercury*, edited by F. Vilas et al., pp. 622–650, Univ. of Ariz. Press, Tucson.

Watt, J. P., G. F. Davies, and R. J. O'Connell (1976), Elastic properties of composite-materials, *Rev. Geophys.*, *14*, 541–563, doi:10.1029/RG014i004p00541.

Weidenschilling, S. J. (1978), Iron/silicate fractionation and the origin of Mercury, *Icarus*, *35*, 99–111, doi:10.1016/0019-1035(78)90064-7.

Weidenschilling, S. J., and J. N. Cuzzi (1993), Formation of planetesimals in the solar nebula, in *Protostars and Planets III*, edited by E. H. Levy and J. I. Lunine, pp. 1031–1060, Univ. of Ariz. Press, Tucson.

Wetherill, G. W. (1988), Accumulation of Mercury from planetesimals, in *Mercury*, edited by F. Vilas et al., pp. 670–691, Univ. of Ariz. Press, Tucson.

Wetherill, G. W. (1994), Provenance of the terrestrial planets, *Geochim. Cosmochim. Acta*, *58*, 4513–4520, doi:10.1016/0016-7037(94)90352-2.

Williams, J.-P., O. Aharonson, and F. Nimmo (2007), Powering Mercury's dynamo, *Geophys. Res. Lett.*, *34*, L21201, doi:10.1029/2007GL031164.

C. R. Bina, Department of Earth and Planetary Sciences, Northwestern University, Evanston, IL 60208, USA.

S. J. Desch, M. A. Riner, and M. S. Robinson, School of Earth and Space Exploration, Arizona State University, Tempe, AZ 85287, USA. (mariner@higp.hawaii.edu)